SECOND EUROPEAN ROTORCRAFT AND POWERED LIFT AIRCRAFT FORUM

Paper No 22

ROTOR RESPONSE PREDICTION WITH NON-LINEAR AERODYNAMIC LOADS ON THE RETREATING BLADE

J.J. Costes

Office National d'Etudes et de Recherches Aérospatiales (ONERA)
92320 Châtillon (France)

September 20-22, 1976

Bückeburg, Federal Republic of Germany

Deutsche Gesellschaft für Luft- und Raumfahrt e.v.

Postfach 510645, D-5000 Köln, Germany

ROTOR RESPONSE PREDICTION WITH NON-LINEAR AERODYNAMIC LOADS ON THE RETREATING BLADE

J.J. Costes

Office National d'Etudes et de Recherches Aérospatiales (ONERA)
92320 Châtillon (France)

Summary

For several years, ONERA has been performing researches with the aim of predicting helicopter blade dynamic response and loads. The application of linearized methods to the prediction of loads on flexible blades has already been illustrated at the first European Forum. The object of the present paper is a calculation taking account of the non-linear aerodynamic loads due to high angle of attack on the retreating blade. The programme is still limited to rigid blades, but its extension to flexible blades offers no theoretical difficulty.

The aerodynamic three-dimensional and compressible effects are taken into account with the acceleration potential method and the effects of large incidence are evaluated with a mathematical model based on airfoil wind tunnel tests and superimposed through an iterative procedure.

The theoretical results have been compared with experimental data obtained on a rotor tested in the large wind tunnel of Modane.

Résumé

Depuis plusieurs années, l'ONERA poursuit des recherches dans le domaine de la prévision des charges aérodynamiques et de la réponse dynamique des pales d'hélicoptères. Une application des méthodes linéaires au calcul des charges pour un rotor à pales souples a déjà été présentée au premier Forum Européen. Le but de la présente étude est l'introduction des non linéarités dues aux incidences élevées présentes dans la zone de la pale reculante. Le calcul est actuellement limité au cas d'une pale rigide articulée, mais l'extension au problème de la pale souple ne présente pas de difficultés théoriques.

Les effets tridimensionnels et ceux dus à la compressibilité sont pris en compte par la méthode du potentiel d'accélération. Les non linéarités induites par les grandes incidences sont incluses par un processus pas à pas à l'aide d'un modèle mathématique fondé sur des résultats expérimentaux bidimensionnels.

La théorie a été comparée à des résultats expérimentaux obtenus dans la grande soufflerie de Modane.

INTRODUCTION

For a few years ONERA has been pursuing researches in the aeroelastic field, with the aim of predicting the in flight vibratory response of a helicopter. The first step has been the development of a computer programme based on the assumption of linear aerodynamics and using the blade normal modes of vibration as degrees of freedom of flexibility.

The validity of this method is restricted to flight cases where the aerodynamic angle of attack on the blade remains small all over the rotor disk. In the method presented in this paper, non linear aerodynamic effects are included, but the blades have been considered as rigid for the sake of simplicity. Even with this simplification, the programme may be used to solve many practical non linear problems where the influence of blade flexibility is small, such is the case for performance.

1 – LINEAR, THREE-DIMENSIONAL COMPRESSIBLE AERODYNAMICS

1.1 – Acceleration potential theory

The method presented here is based on the acceleration potential or doublet theory, Ref. (1), (2), (3). The blade is assimilated to a surface of pressure discontinuity. We assume that the blade motion is known.

For a prescribed distribution of pressure discontinuity defined by a function of the space coordinates (over the blade surface) and time (from the remote time $t = -\infty$ to the present time $t = t_o$), one is able to calculate, by integration of a rather complicated kernel function, the total induced velocity, resulting from the attached and shed vortices, at any given point and time t_o. The formulation differs fundamentally from the vortex theory which determines the velocity induced by the shed vortices instead of the total velocity.

On the blade surface the normal component of this total induced velocity is a known function of time also named downwash. It is given by the non-separation condition. Such a condition introduces a relation between the pressure discontinuity and the blade movement. This condition is directly used to compute the lift forces on the blades without necessitating any two-dimensional assumption such as the one used in Prandtl method.

1.2 – Practical application of the theory

In order to save computer time, one is obliged to simplify the problem, Ref. (4) and (5). The following assumptions are introduced.

1) The blade movement is a known periodical function of time.

2) The blade is represented by a lifting line located on the 25 per cent chordwise position.

3) The non separation condition is applied on the 75 per cent chordwise position.

4) The lift is supposed to be a linear combination of prescribed functions of time and blade radius, according to the following formula :

$$(1)\quad F(r,t) = \sqrt{1-\eta^2}\left\{\sum_{i=1}^{n} Z_i L_i(r) + \sum_{i=1}^{n}\sum_{j=1}^{m} X_{ij} L_i(r)\cos j\psi + \sum_{i=1}^{n}\sum_{j=1}^{m} Y_{ij} L_i(r)\sin j\psi\right\}$$

where $L_i(r)$ is a Lagrange polynomial,

ψ is the azimuthal angle on the rotor disk, with the origin on the backward blade position,

$\eta = \dfrac{2r - R_1 - R_0}{R_1 - R_0}$

r : radial coordinate of a blade section

R_0 radial coordinate of the blade root

R_1 radial coordinate of the blade tip

Z_i X_{ij} Y_{ij} unknown coefficients, to be determined by application of conditions 1 and 3.

For most of the computations n = 5 and m = 6 and there is a total of 65 unknown coefficients (Z, X, Y).

The first step of the method is to compute by a time integration the total induced velocity generated by each lift function

$L_i(r)$
$L_i(r)\cos j\psi$
$L_i(r)\sin j\psi$.

There is a total of 65 such functions and the integration is performed for each function on 65 points P_0, evenly distributed on the rotor disk. As a consequence of the linear aerodynamics, the induced velocity is the sum of the velocities induced by each function with the appropriate coefficient Z_i, X_{ij} or Y_{ij}. The relation between the velocity at the points P_0 and the set of coefficients gives algebraic equations which can be written in the matrix form :

$$(2)\quad \begin{bmatrix} & A & \end{bmatrix} \begin{bmatrix} Z_{ij} \\ X_{ij} \\ Y_{ij} \end{bmatrix} = \begin{bmatrix} W \end{bmatrix}$$

where [A] is the matrix resulting from the integration : each coefficient of A gives the velocity induced at a particular point by a particular prescribed lift function ;

$\begin{bmatrix} Z_i \\ X_{ij} \\ Y_{ij} \end{bmatrix}$ is the column of the unknown coefficient ;

[W] is the column of the total induced velocity for each point P_0. If the condition 1 is assumed, W is known and obtained by projection of the blade velocity on the normal to the blade local skeleton.

The resolution of the linear system (2) gives the coefficients Z, X, Y, and by application of (1), the lift distribution on the rotor disk is obtained.

1.3 — Introduction of the aerodynamic incidence

One can notice that, so far, the incidence has not been introduced, of course we need to know the feathering angle along the blade as well as the cyclic and collective pitch. These angles determine the section geometric position refered to a conventional plane. The forces are directly obtained by solving the linear system (2). Then one can assume that the lift is created on each blade section as on an airfoil in a two-dimensional flow. The blade local incidence is the value of incidence which would give the same local lift on the airfoil. This procedure is based on the same assumptions as the Prandtl's method.

Now let us compare the calculation procedures used with the doublet method and with the vortex method in a block diagram.

(See Table 1).

When the doublet method has given the aerodynamic forces, the determination of the Prandtl's incidence is based on the following formula :

$$(3)\quad \alpha_p = \frac{F\sqrt{1-M^2}}{2\pi\rho V_n^2\, b}$$

where F is the lift by unit spanwise length in N/m,
V_n is the local normal velocity to the blade m/sec,
$M = V_n/a$ local Mach number, a sound velocity,
b half chord.

This is a very simple quasi steady formula but which can give satisfactory results for the low reduced frequencies usually met on helicopter rotors. The incidences thus obtained are used to predict the drag and stall.

Table 1.

VORTEX METHOD gives velocity induced by shed vortices	→ Feathering angle + shed vortices induced velocity gives Prandtl's incidences	→ Prandtl's incidence gives aerodynamic forces
DOUBLET METHOD gives *the velocity resulting from the* shed and attached vortices	→ Feathering angle + sum of shed and attached vortices induced velocity gives forces on the blade	→ Forces on the blade gives *two-dimensional Prandtl's* incidence

2 – NON LINEAR COMPRESSIBLE AERODYNAMICS

2.1 – Introduction of the effective Prandtl's incidence (see Ref. (6))

Let us assume that the method of paragraph 1 has been used to compute the linear forces F and Prandtl's incidences α_p, on the rotor disk. If α_p is no longer small, separation can occur. The blade will experience unsteady stall. The actual forces on the blade, as one can measure by pressure transducers and a chordwise integration is noted $\bar{F}(r, t)$. Relation (4) is verified

$$(4) \qquad \left|\bar{F}(r, t)\right| \leq \left|F(r, t)\right|$$

An interpretation of $\bar{F}(r, t)$ can be given by saying that the local profile has the effective incidence α_{Peff} (fig. 1). This incidence is derived from $\bar{F}(r, t)$ with a formula similar to (3) :

$$(5) \qquad \alpha_{Peff} = \frac{\bar{F}(r, t)\sqrt{1 - M^2}}{2\pi\rho V_n^2 \, b}$$

by comparison of (3), (4), (5), one has :

$$(6) \qquad \left|\alpha_{Peff}\right| \leq \left|\alpha_p\right|.$$

The difference $(\alpha_p - \alpha_{Peff})$ can be assimilated to a loss of incidence due to stall.

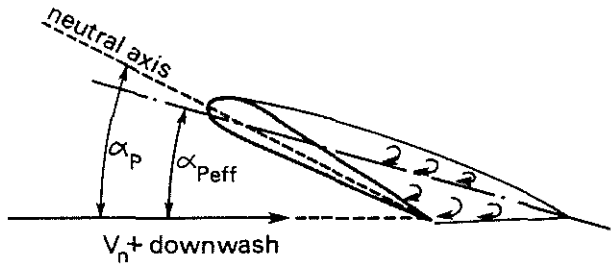

Fig. 1 – Effective aerodynamic incidence for a stalled profile.

2.2 – Grass and Harris' method

In order to solve the problem, a relation is needed between α_{Peff} and α_p. Because of the unstationary character of stall on the rotor disk, one can expect that, at the present time t_o, the incidence $\alpha_{Peff}(t_o)$ is determined by all the time history of $\alpha_p(t)$ from $-\infty$ to t_o. This relation can be given by experiment or by any available method. A simple method, developped at the Boeing Company has been used in the computer program. The time dependance is restricted to the values of both the incidence and the incidence first derivative. Thus we have :

$$(7) \qquad \alpha_{Peff}(t_o) = f\left(\alpha_p(t_o), \dot{\alpha}_p(t_o)\right)$$

f is a non linear function of the variables α_p and $\dot{\alpha}_p$. Determinations of the relation (7) is given in Ref. (9) and (6). For a simple sinusoidal variation of $\alpha_p(t)$, one obtains a lift coefficient $C_z(t)$ roughly centered on the static experimental C_{zo} curve (fig. 2).

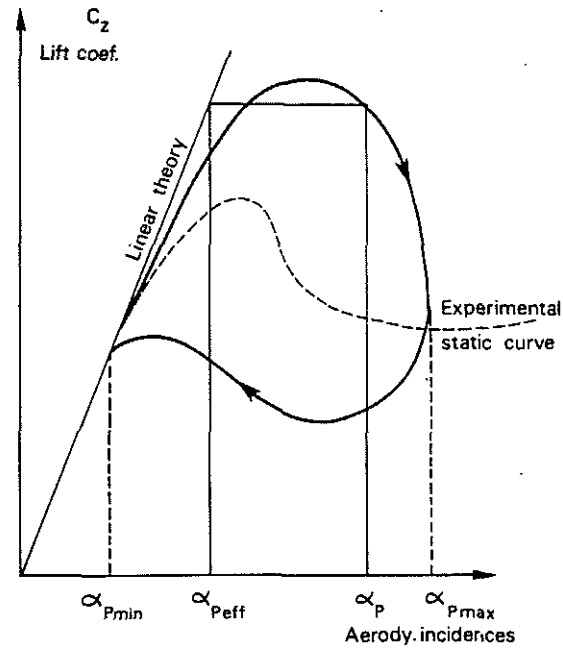

Fig. 2 – Experimental C_Z loop for a sinusoidal variation of α_p.

2.3 – Physical assumptions

As it has been shown in the linear case, the forces on the rotor disk are determined by a condition which express the fact that the velocity of the fluid is tangent to the local profile neutral axis. This is no longer true when separation occurs. It will be supposed that one can replace the actual profile by a new one, the neutral axis of which makes , with the former one, an angle equal to the loss of incidence. Besides, it is assumed that the wake induced velocities are still determined by the same linear relations as formely, except for the fact that non linear lift forces replace the former linear ones. The problem is thus brought back to the precedent linear one expressed by relation (2) with the important difference due to the presence of an unknown right hand term. This right hand term can be considered as the velocity normal to the equivalent neutral axis of the stalled profile. It is now possible to imagine a step by step method to compute the non linear forces. At the first step, the linear solution give the value of α_p, then with the non linear relation (7) one obtains the effective incidence α_{Peff}, which in turn gives a new right hand term and a new value for the forces and so on. The problem is equivalent to solving a non linear systems of 65 equations with 65 unknown parameters.

2.4 – Resolution of the non linear system

For convenience, the aerodynamic incidences α_p are chosen as the unknown parameters to be determined at the 65 points P_o of the rotor disk. Once the incidences are determined the relation (7) gives α_{Peff} and (5) provides the actual non linear forces $\bar{F}$ on the 65 points P_o. All over the rotor disk the interpolation of $\bar{F}(r, \psi)$ is made according to formula (1) as for the linear computation. Because of the large number of unknown parameters α_p (currently 65), the method used is a Newton's generalized one which converges fast enough if the non-linearities are not too severe. The starting point is provided by the solution of the associated linear system. The convergence is likely to be difficult for strongly non linear cases, that is to say for heavily stalled rotors. Fortunately the stalled region remains restricted to the side of the retreating blade ; this in fact reduces the number of non linear equations.

3 – AERODYNAMIC FORCES AND BLADES MOVEMENT COUPLING

3.1 – *Solution of the complete problem*

So far, in paragraphes 1 and 2, the blade movement has been considered as known in function of time. It remains to express the blade mechanical equilibrium. The problem has already been solved with linear aerodynamics for an articulated flexible blade Ref. (7) (8). Here, it will be restricted to a rigid flap and lead-lag hinged blade without hub movement. The Lagrange's equation express the coupling between blade mechanical movements and aerodynamic forces. If the blade angular movements are supposed small and if moreover the drag forces are neglected or added as known forces, then the Lagrange's equations are linear. By an inversion matrix technique one can solve the system and obtain the blade periodical movement as a linear function of the unknown 65 lift coefficients $\bar{F}$. By combination of this result with the non linear aerodynamic system of paragraph 2, a new non linear system is obtained, which governs the response of the fully coupled aerodynamic and mechanical system. The small non linearities introduced by large blade movements and drag forces are taken into accounts as correction coefficients in a step by step computation. Fortunately, these non linearities are small and do not introduce convergence difficulties as the strongly non linear system of paragraph 2 can do.

Eventually the solution of the problem is given by two step by step computation procedures. The convergence needs a rather long computer time, about 8 minutes of UNIVAC 1110. (Acceleration potential induced velocities not included).

4 – APPLICATIONS

4.1 – Choice of one experiment performed at the Modane test rig

The computation method presented in the preceding paragraphs has been compared with experimental results obtained in July 1970 in the S1 large wind tunnel of Modane. The model was a very rigid flap and lead-lag articulated one, with a diameter of 4.15 m and a blade chord of 0.21 m. In flight measurements with pressure transducers along 4 blade sections provide, by integration, the lift at reduced distances $r/R = 0.52$; 0.71 ; 0.855 ; and 0.952 from the rotor axis. The blade inertia coefficients have been measured in a ground experiment to be used in the Lagrange's equations. The flight case selected for comparison is a heavily stalled one at an avance ratio $\mu = 0.3$. The angle α_q between the shaft axis and the perpendicular to the flight path is $\alpha_q = -15.94°$. The feathering angle at 75% of blade spanwise location is 13.49°. There is no cyclic pitch ; the control is provided by the variation of the angle α_q. The rotor is operating at $C_T/\sigma = 0.1138$; $C_L/\sigma = 1.728$; $\Omega R = 200$ m/sec at the tip. The blade flapping movement is approximated by the formula :

$$\beta(t) = \beta_0 + \beta_{C1}\cos\psi + \beta_{S1}\sin\psi + \ldots + \beta_{C6}\cos 6\psi + \beta_{S6}\sin 6\psi$$

and the lead-lag movement by :

$$\theta(t) = \theta_0 + \theta_{C1}\cos\psi + \theta_{S1}\sin\psi + \ldots + \theta_{C6}\cos 6\psi + \theta_{S6}\sin 6\psi$$

4.2 – Incidence and lift charts

For the flight configuration considered, fig. 3 and 4 show the charts of incidence for linear and non linear calculations. In both figures it is worth to notice the 0 incidence occuring at both ends of the lifting surface. On the reverse flow area boundary the incidence is ± 90°. At the blade tip there very large incidence variation on most of the rotor disk. This is mainly an effect of the tip vortex. Both charts are very similar in their general shape. Nevertheless differences occur in the retreating side region. This is clearly shown on figure 5 for the $\alpha_p = 15°$ contour. The area embraced by the contour is much larger in the non linear case, in spite of the lower forces (fig. 6 and 7). This is the consequence of a complex combined effect of blade movement and induced velocities, different in both cases. The differences for the 1° and 2° contours have no important effect on the lift forces. They are induced by the very small incidence slope on the $\psi = 90°$ advancing blade region.

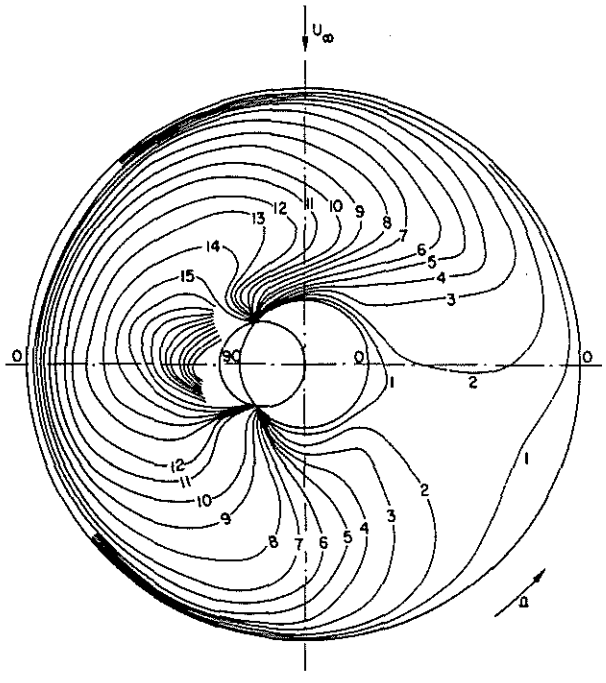

Fig. 3 – Map of incidence linear computation.

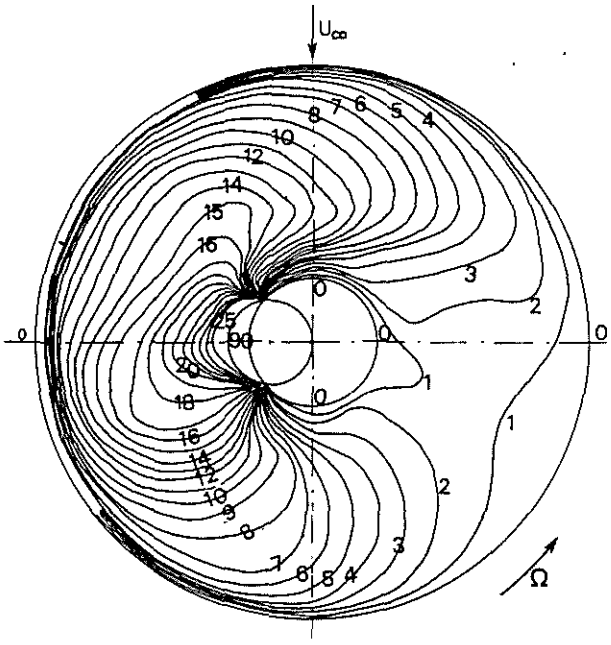

Fig. 4 – Map of incidence nonlinear computation.

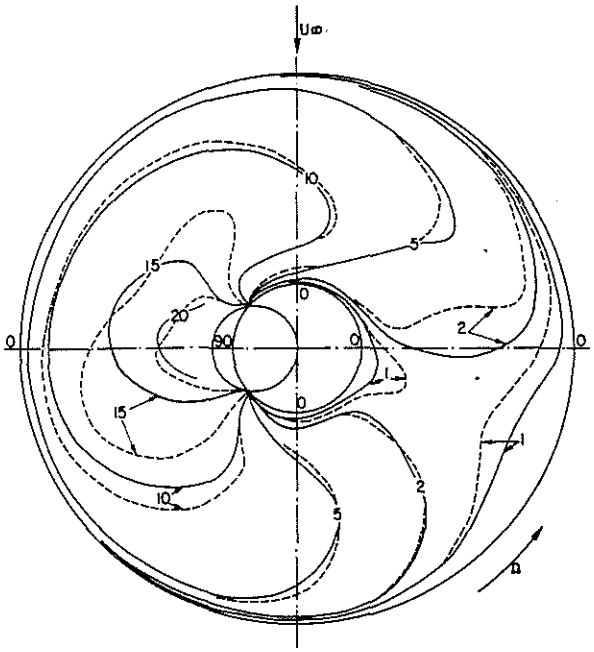

Fig. 5 — Comparison of incidences obtained by linear and nonlinear computation.
——— linear computation fig. 3
— — — nonlinear computation fig. 4

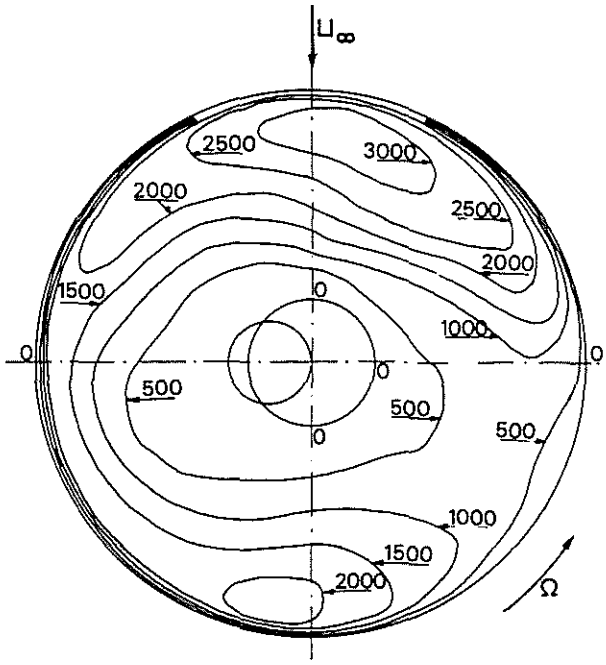

Fig. 7 — Lift (N/m) map. Nonlinear computation.

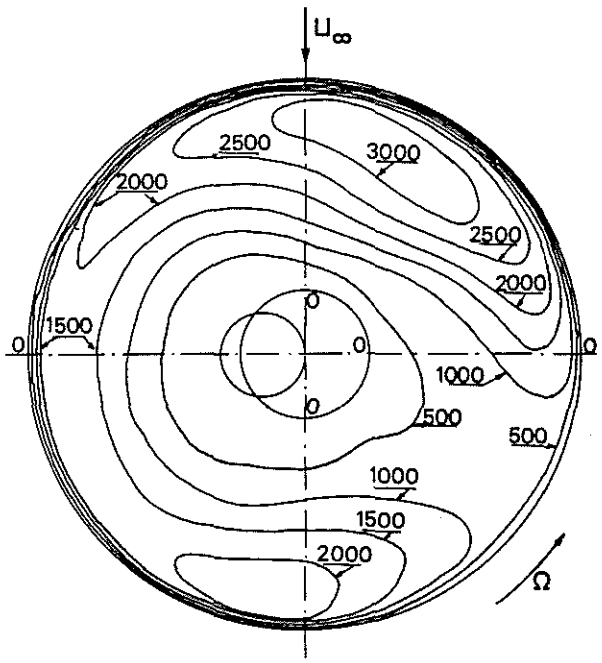

Fig. 6 — Lift (N/m) map. Linear computation.

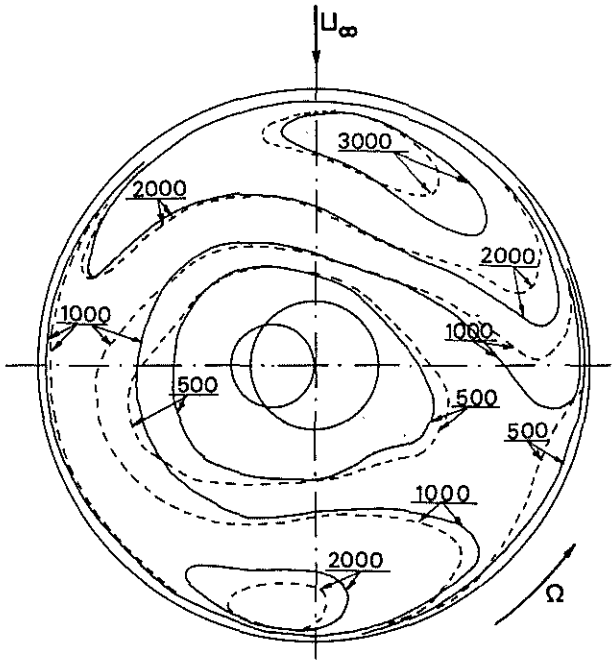

Fig. 8 — Comparison of lift (N/m) obtained by linear and nonlinear computations.
——— linear computation fig. 6
— — — nonlinear computation fig. 7

The forces on the rotor disk are presented on figs. 6, 7, 8 ; they show the expected decrease in lift induced by the non linear effects. It is important to notice that the highest lift occurs on both the forward and backward parts of the rotor disk.

4.3 — Comparison with experiment

The time histories of lift are given in fig. 9, 10, 11, 12. They result from the integration of 10 pressures transducers located on 4 radial locations. The results of the experiment and the linear and nonlinear computations are given in a normalized form : $F = \int_{chord} \frac{\Delta p}{Po} \frac{dx}{c}$

where Δp is the pressure difference between intrados and extrados ; Po is the static pressure in the wind tunnel.

Non linear computation shows some improvement at sections r/R = 0.52 ; 0.71 ; 0.855. At the blade tip, where the incidence is small, both computations are similar. The difference with experiment can be due to non linear effects of the large incidence spanwise variation or to radially swept flow in

the stalled region.

Figure 13 is the comparison between experiment and computations for the harmonic analysis of lift. Non linear results are generally in better agreement with experiment.

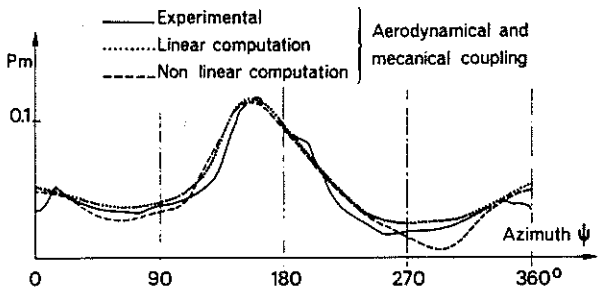

Fig. 9 — Time history of normalized lift force at radial section r/R = 0.520.

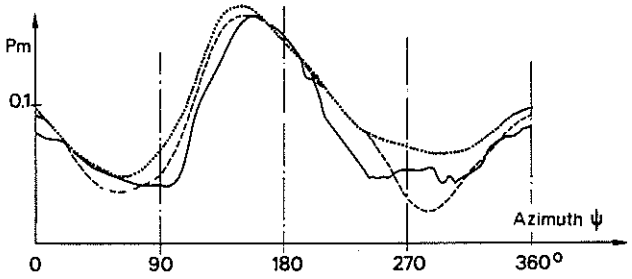

Fig. 10 — Time history of normalized lift force at radial section r/R = 0.710.

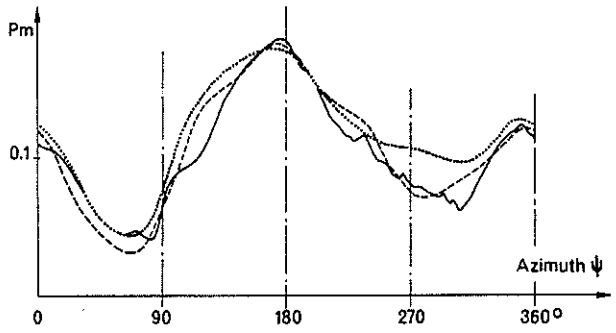

Fig. 11 — Time history of normalized lift force at radial section r/R = 0.855.

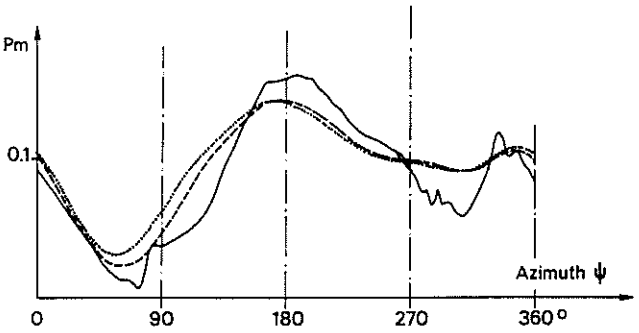

Fig. 12 — Time history of normalized lift force at radial section r/R = 0.952.

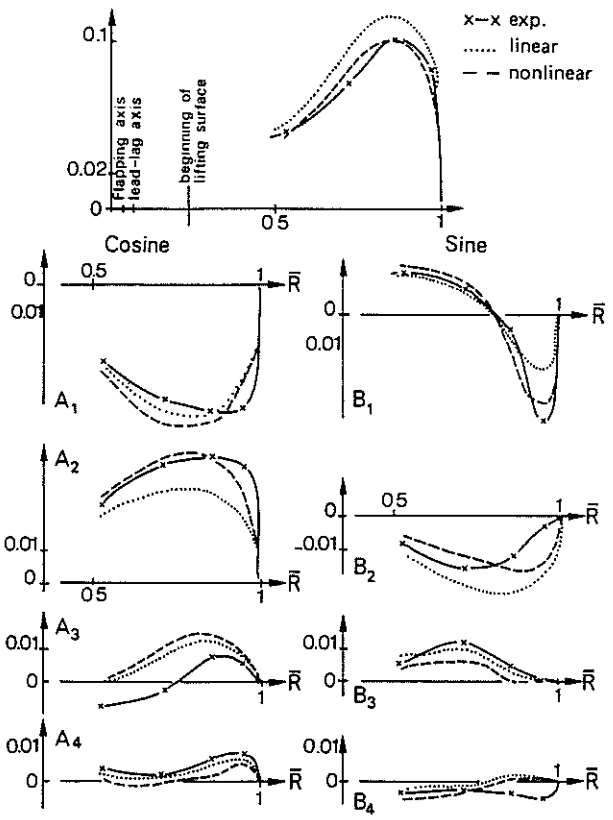

Fig. 13 — Harmonic analysis of normalized lift.

4.4 — Effect of multicyclic control

As one can observe on fig. 7, the maximum lift occurs on both front side and rear side of the rotor disk. The forces remain small at $\psi = 90$ and $\psi = 270°$. If the lift could be made even smaller at the azimuth $\psi = 270°$, one can expect that the stall would be avoided or at least deleted. To obtain this effect would require a maximum of the feathering angle at $\psi = 0°$ and $\psi = 180°$ and a minimum at $\psi = 90°$ and $\psi = 270°$. This leads to a cosine second harmonic multicyclic pitch angle. To have an idea of the effects one can expect, a tentative computation has been carried out with a 5° second harmonic cosine term. There is no first harmonic pitch and control of lift and thrust is obtained by tilting the shaft axis and adjusting the general pitch angle. Calculation have shown a small decrease of both α_q and the general pitch, but a 7.5% increase of the power required to turn the rotor and a small increase in the vibratory level at the rotor head (see figure 14). Nevertheless the incidence charts (fig. 15 and 16) show a very important variation of the contour lines and a substantial decrease of the incidence at azimuth $\psi = 270°$. This may in turn decrease the stall induced pitching moment on the blade but their calculation has not been included in the computer program so far. Figure 17 shows the maximum of aerodynamic incidence on the rotor disk, experimented by a profile, and the decrease due to multicyclic control. The new force distribution is given on figure 18.

	No multicyclic pitch	Multicyclic pitch 5° x cos2ψ
Collective pitch	13.49°	12.465°
α_q	15.94°	13.24°
Thrust	444.41 N	442.37 N
Lift	4 582.34 N	4 574.79 N
Power required	113,939 watts	119,250 watts
Blade coning	1.34°	1.37°
1st harmonic cosine flapping mvt	9.58°	6.32°
1st harmonic sine flapping mvt	0.06°	0.575°
2nd harmonic cosine flapping mvt	0.183°	0.40°
Mean inplane lagging angle	− 1.72°	− 1.80°

Fig. 14 — Effects of multicyclic pitch motion (angle α_q and collective pitch adjusted to obtain the same thrust and lift).

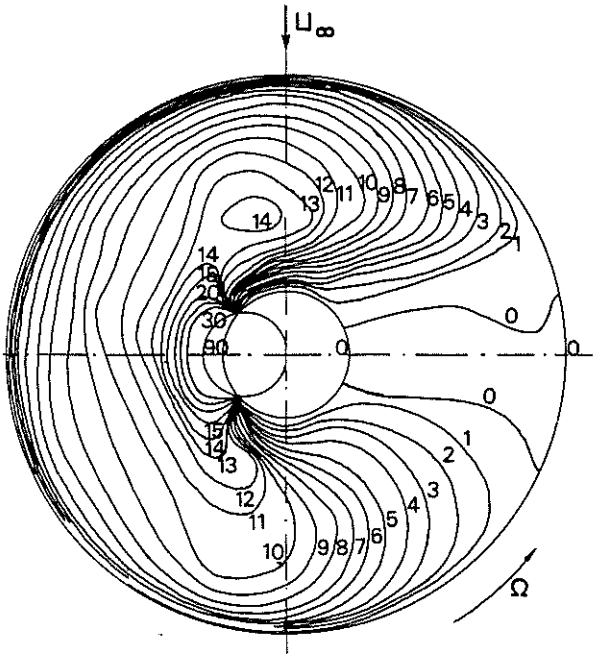

Fig. 15 — Incidences map. Nonlinear computation 5°cos2ψ multicyclic pitch.

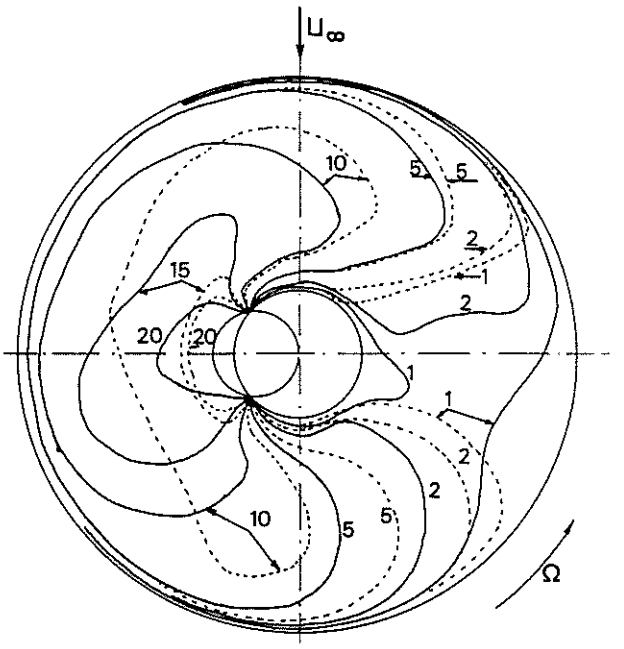

Fig. 16 — Comparison of incidences maps.
——— nonlinear computation no multicyclic pitch
– – – nonlinear computation 5°cos2ψ multicyclic pitch.

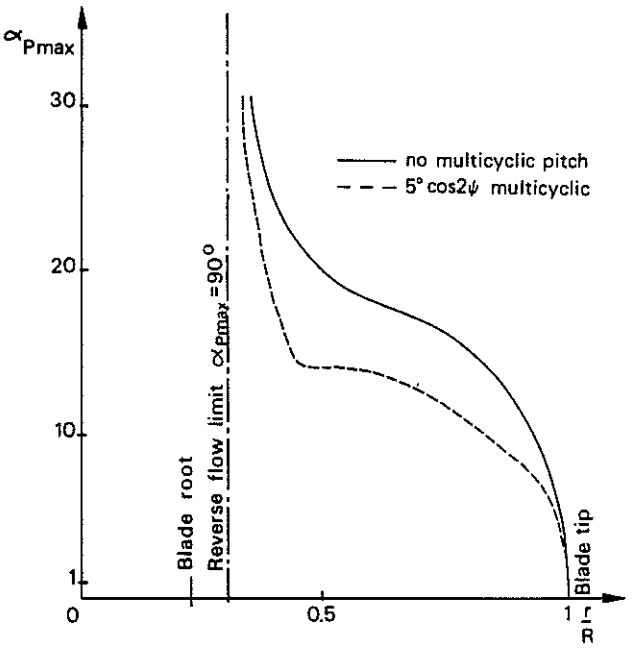

Fig. 17 — Maximum of incidence along blade.

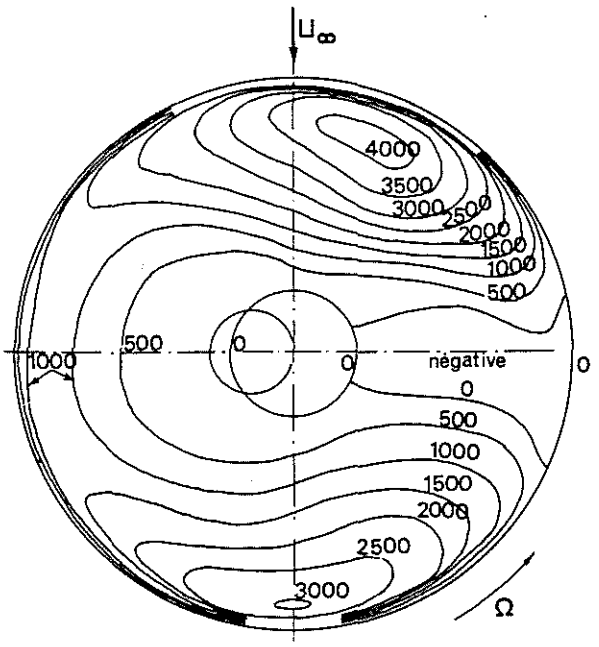

Fig. 18 – Map of lift forces. Nonlinear computation $5° cos2\psi$ multicyclic pitch.

5 – CONCLUSION

The computer program presented in this paper is restricted to the case of a rigid articulated rotor. Lift non linearities due to stall are included, but the important pitch moment variation expected in such flight regime has been omitted. This is an important limitation which can only been removed by further development of both two-dimensional experiments and tridimensional theory. More experimental results are also needed to explore Reynolds numbers effect and full use of all possibilities of the theory.

References

1 Williams D.E. – "Three dimensional subsonic theory" AGARD, Manual on Aeroelasticity. Vol. II.

2 Dat R. and Akamatsu Y. – "Représentation d'une aile par des lignes portantes ; Application au calcul de l'interaction de deux ailes tandem". AGARD C.P. No 80, Part 1, No 5 (1971).

3 Dat R. – "Représentation d'une ligne portante animée d'un mouvement vibratoire par une ligne de doublets d'accélération." La Rech. Aérosp. No 133 (nov-déc 1969). Traduction NASA TT.F 12952 (1970).

4 Dat R. – "La théorie de la surface portante appliquée à l'aile fixe et à l'hélice". La Rech. Aérosp. No 1973-4 (juillet-août). Traduction ESRO-TT-90 (1974).

5 Costes J.J. – "Calculs des forces aérodynamiques instationnaires sur les pales d'un rotor d'hélicoptère". La Rech. Aérosp. No 1972-2 (mars-avril). Traduction NASA-TT-F-15039 (1973). See also AGARD Report No 595.

6 Costes J.J. – "Introduction du décollement instationnaire dans la théorie du potentiel d'accélération. Application à l'hélicoptère". La Rech. Aérosp. No 1975-3.

7 Tran Cam Thuy, Twomey W., Dat R. – "Calcul des caractéristiques dynamiques d'une structure d'hélicoptère par la méthode des modes partiels" La Rech. Aérosp. No 1973-6 (nov-déc.).

8 Tran Cam Thuy, Renaud J. – "Theoretical predictions of aerodynamic and dynamic phenomena on helicopter rotors in forward flight". First European Rotorcraft and Powered Lift Aircraft Forum. 22-24 sept. 1975.

9 Gormont R.E. – "A mathematical model of unsteady aerodynamics and radial flow for application to helicopter rotors" USA-AMRDL TR 72-67 (mai 1973).

10 Hammond C.E., Runyan H.L. and Mason J.P. – "Application of unsteady lifting surface theory to propellers in forward flight". AIAA paper No 74-419.

11 Hille R. – "Erweiterung des Traglinienmodells beim Hubschrauberrotor". Institut für Schiffbau der Universität Hamburg, Bericht Nr 315, Sept. 1974.

12 Rebuffet P. –"Aérodynamique expérimentale" Béranger, Paris, 1962.